

Learning Quadrupedal Locomotion via Differentiable Simulation

Clemens Schwarke, Victor Klemm, Jesus Tordesillas, Jean-Pierre Sleiman, and Marco Hutter

Abstract—The emergence of differentiable simulators enabling analytic gradient computation has motivated a new wave of learning algorithms that hold the potential to significantly increase sample efficiency over traditional Reinforcement Learning (RL) methods. While recent research has demonstrated performance gains in scenarios with comparatively smooth dynamics and, thus, smooth optimization landscapes, research on leveraging differentiable simulators for contact-rich scenarios, such as legged locomotion, is scarce. This may be attributed to the discontinuous nature of contact, which introduces several challenges to optimizing with analytic gradients. The purpose of this paper is to determine if analytic gradients can be beneficial even in the face of contact. Our investigation focuses on the effects of different soft and hard contact models on the learning process, examining optimization challenges through the lens of contact simulation. We demonstrate the viability of employing analytic gradients to learn physically plausible locomotion skills with a quadrupedal robot using Short-Horizon Actor-Critic (SHAC), a learning algorithm leveraging analytic gradients, and draw a comparison to a state-of-the-art RL algorithm, Proximal Policy Optimization (PPO), to understand the benefits of analytic gradients.

I. INTRODUCTION

Today’s RL algorithms rely on sampling the task objective in order to estimate the gradient of the objective with respect to the parameters of the control policy. This Zeroth-order Gradient (ZoG) estimation allows for optimization over nondifferentiable functions, which has been crucial for its applicability within robotics, as physics simulators are typically not differentiable. Recently, several differentiable simulation frameworks have been proposed, opening up the possibility to compute the derivative of the dynamics analytically. Gradients derived from such simulations can potentially enhance sample efficiency by offering less variance than ZoG estimates [1].

Nevertheless, employing FoGs presents numerous challenges that have so far restricted their effective use, particularly in complex, contact-rich learning tasks like legged locomotion [2], [3], [4]. The primary obstacles introduced by contact are discontinuous optimization landscapes and discretization artifacts. While research has been focusing on addressing the challenges from the algorithmic perspective, little work studies the impact of different simulation techniques. We aim to assess the role of the simulator by exploring the effect of different contact models on the learning process and on the quality of the learned behaviors. We probe a simple spring-damper model, similar to the models in [5], [6], that provides useful gradients but yields

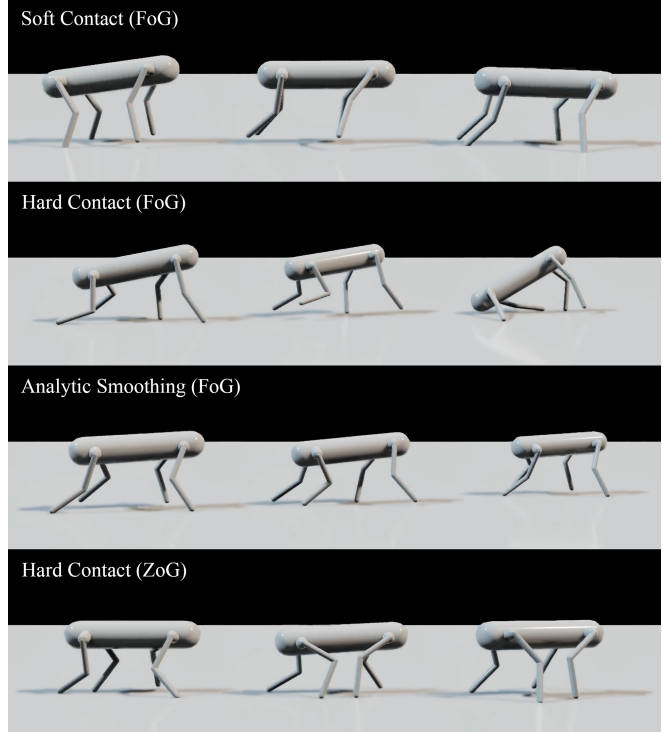


Fig. 1: A 12 Degree of Freedom (DoF) quadrupedal robot learning to locomote on flat terrain in a differentiable simulation. Policies trained with First-order Gradients (FoGs) and soft contact exhibit hopping behaviors (top left). When training with FoGs and hard contact, policies follow unreasonable foothold patterns, sometimes leading to failure (top right). Policies trained with ZoGs and hard contact or with FoGs and the analytically smooth contact model exhibit effective and stable locomotive gaits (bottom). Learned behaviors can be seen in the supplementary video: <https://youtu.be/wmyp76Y5mPg>.

limited physical accuracy against a hard contact model based on Moreau’s time-stepping scheme [7], that offers more accurate physics but less informative gradient signals.

Additionally, we adopt the idea of replicating the effect of stochastic smoothing found in current RL algorithms [8] and propose a smooth contact model that yields informative gradients while producing physically realistic locomotion behaviors. The model remains stable across any stiffness level and allows for large time steps, overcoming the limitations of traditional soft contact models.

We showcase the feasibility of attaining physically realistic locomotion skills utilizing analytic gradients with a quadrupedal robot, illustrated in Fig. 1, and compare the first-

All authors are with the Robotic Systems Lab, ETH Zürich, Switzerland. Mail: {cschwarke, vklemm, jtordesillas, jsleiman, mahutter}@ethz.ch

order-based algorithm SHAC [5] to PPO [9], a RL algorithm that has shown impressive results in the legged locomotion domain [10].

In summary, our main contributions are:

- An evaluation of different contact models and their effects on optimization
- A smooth contact model that combines the advantages of soft and hard contact modeling
- A demonstration of achieving physically plausible locomotion skills through analytic gradients¹
- A comparison of SHAC and PPO using our simulation, highlighting the benefits of analytic gradients

II. RELATED WORK

Motivated by the availability of Automatic Differentiation (AD) tools, many differentiable simulators, summarized in Tab. I, have been developed in recent years. One of the first simulators amenable to AD is presented in [2]. Attempts to optimize a locomotion policy for an 8 DoF quadruped result in suboptimal behaviors involving front flips, yet they establish the feasibility of leveraging differentiable simulations for learning. Subsequently, [11] presents an analytic solution to the Linear Complementarity Problem (LCP) of contact. The simulator Nimble [12] exploits the sparse nature of the LCP to increase computational efficiency and leverages symbolic differentiation instead of AD.

DiffTaichi [3] bypasses the need to differentiate the LCP with an impulse-based 2D simulation for rectangles. The authors point out the importance of Time of Impact (ToI) estimation for optimization convergence. Warp [13], a Python-based, differentiable kernel programming framework, includes two simulation routines for rigid-body dynamics, relying on XPBD [14] and a soft contact model. It facilitates fast computation through GPU parallelization and source code transformation to CUDA. Brax [4], a simulator built on the JAX library, follows a similar approach and has been continuously expanded to include various simulation pipelines, like MuJoCo [15] and PBD. The accompanying publication includes experiments for locomotion tasks but reports that optimizing with analytic gradients does not yield locomotive gaits.

TABLE I: Differentiable Rigid-Body Simulators

Name	Differentiation	Contact Modeling	Device
Nimble [12]	Symbolic	LCP	CPU
DiffTaichi [3]	Automatic	Impulse-based	GPU
Warp [13]	Automatic	XPBD, Soft	GPU
Brax [4]	Automatic	MuJoCo, PBD, Soft	GPU
Dojo [16]	Symbolic	NCP	CPU

Dojo [16] prioritizes physical accuracy over speed, solving the Nonlinear Complementarity Problem (NCP) of contact

¹To the best knowledge of the authors, this was achieved for the first time, as previous attempts either leveraged spring-based contact [5] or non-standard locomotion such as frontflips [2].

with an interior-point method and using variational integrators for energy conservation. It utilizes intermediate solver iterations for gradient computation, aiding in optimization, but it suffers from slow CPU execution and lacks support for parallelism, limiting its use in RL contexts.

The benefits of optimizing with FoGs have been reported for various applications, such as soft body manipulation [17], system identification from video [18], [19], or grasp synthesis [20]. However, despite promising results, FoG-based methods face several challenges.

To overcome the tendency to stagnate in local minima, [21] combines Bayesian optimization with local Gradient Descent (GD) steps. The authors examined multiple simulators including DiffTaichi [3], Nimble [12], and Warp [13], and found the provided gradient quality to hinder optimization. Grasp²D [20] attempts to improve gradient quality by smoothing collision geometries defined as signed distance fields. However, experiments show that the improvement is moderate. The work also introduces the idea of “leaky gradients,” which allow for informative gradients in the absence of contact. Another approach to dealing with uninformative gradients is presented in [22], introducing “bundled gradients”, defined as the expectation of the gradient under stochastic noise. In a subsequent publication [8], the authors formulate analytically smooth dynamics that mimic the randomized smoothing effect of bundled gradients on nonsmooth dynamics to avoid the need for sampling.

Other works focus on the issue of diverging gradients when computing gradients via Backpropagation Through Time (BPTT), introducing alternatives to differentiating the entire task trajectory. In [23], the authors propose to train a concurrent controller that outputs a series of actions for multiple time steps in the future. This way, the gradient does not have to be propagated through the policy network multiple times. PODS [24] takes a different approach and optimizes the actions taken at each time step. The control policy is then trained on the optimized actions in a supervised fashion.

Instead of entirely relying on FoGs, some works investigate how FoGs can be combined with ZoGs. For instance, [25] uses FoGs to generate additional samples for the critic training of an actor-critic RL algorithm. In [1], an adaptive interpolation scheme combines the two types of gradients depending on their bias and variance. Recently, [5] developed an actor-critic algorithm, SHAC, that leverages FoGs while maintaining a similar structure to current RL algorithms, thus facilitating its integration into standard RL training environments. Short-Horizon Actor-Critic (SHAC) surpasses the performance of purely ZoG-based algorithms, especially for high-dimensional optimization spaces, and successfully optimizes a locomotion policy for MuJoCo’s ant environment [15]. This development presents a promising avenue for the utilization and further exploration of FoGs for complex learning tasks.

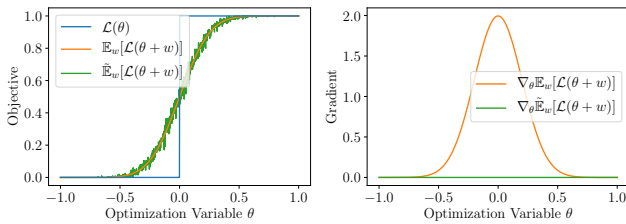


Fig. 2: A deterministic objective $\mathcal{L}(\theta)$ and its expected value $\mathbb{E}_w[\mathcal{L}(\theta + w)]$ under stochastic noise w (left). The approximation $\tilde{\mathbb{E}}_w[\mathcal{L}(\theta + w)]$ is an unbiased estimator of the true expected value. The gradient approximation of the expected value $\nabla_\theta \tilde{\mathbb{E}}_w[\mathcal{L}(\theta + w)]$ is biased if \mathcal{L} is discontinuous (right). A comprehensive analysis of this phenomenon, including discussion of variances, is given in [1].

III. OPTIMIZATION THROUGH CONTACT

FoG-based optimization becomes challenging when the objective function is nonsmooth or discontinuous. To understand the effect of discontinuities on the optimization process, consider a generic optimization problem

$$\min_{\theta} \mathcal{L}(\theta), \quad (1)$$

where \mathcal{L} is the objective or loss function and θ is the optimization variable. ZoG-based algorithms like PPO sample \mathcal{L} stochastically to construct a gradient estimate, effectively optimizing

$$\min_{\theta} \mathbb{E}_w[\mathcal{L}(\theta + w)] = \min_{\theta} \int_w p(w) \mathcal{L}(\theta + w) dw, \quad (2)$$

a stochastic version of the original objective, where w is a stochastic disturbance and $p(w)$ is its probability distribution. Under a finite number of samples, the true expectation is approximated by

$$\tilde{\mathbb{E}}_w[\mathcal{L}(\theta + w)] = \frac{1}{N} \sum_{n=0}^N \mathcal{L}(\theta + w_n) \quad (3)$$

with $w_n \sim p(w)$. Fig. 2 shows that introducing stochasticity smooths discontinuities, explaining the success of RL even in discontinuous scenarios. Applying the same idea in the gradient domain yields

$$\nabla_\theta \tilde{\mathbb{E}}_w[\mathcal{L}(\theta + w)] = \frac{1}{N} \sum_{n=0}^N \nabla_\theta \mathcal{L}(\theta + w_n), \quad (4)$$

which does not accurately approximate the gradient of the stochastic objective in the presence of discontinuities. Instead, the sampled gradient is biased and does not contain useful information, as depicted in Fig. 2. The benefit of stochastic smoothing for ZoG estimation does thus not directly transfer to FoGs.

Even without discontinuities, stiff dynamics may lead to what [1] refers to as empirical bias, apparent under a small number of samples N . Intuitively, if an objective function changes very quickly in a small interval and is constant everywhere else, the gradient computed using Equation 4

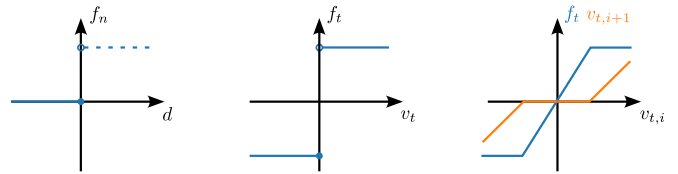


Fig. 3: The discontinuities of hard contact. The normal contact force f_n is discontinuous at a penetration depth d of 0 between two rigid objects. The dashed line indicates that interpenetration does not occur in continuous time (left). The tangential force f_t is discontinuous at a tangential velocity v_t of 0 (middle). In discrete time, the contact force is computed to be applied over the entire time step, resolving the discontinuity. The tangential velocity at the next time step $v_{t,i+1}$ will be 0 until the friction force would need to be exerted for more than one time step (right).

might still yield zero almost everywhere, similar to the FoG shown in Figure 2, if none of the sampled gradients encounter the steep ascent.

A. Contact Discontinuities

Rigid-body simulators often employ hard contact models because they allow for large simulation time steps, do not require parameter tuning, and model physics with high fidelity. Inconveniently, hard contact models introduce discontinuities to the continuous-time dynamics. First, contact forces are only present if two objects are in contact, causing a discontinuity with respect to the contacting object's positions. Second, assuming a Coulomb friction model, tangential contact forces switch direction discontinuously if the tangential contact velocity changes direction.

Interestingly, the discontinuity introduced by the Coulomb friction model is not present in discrete-time simulation because the frictional force f_t is assumed to act over an entire time step. If the tangential contact velocity $v_{t,i}$ is small enough, the Coulomb friction force only needs to act over part of the time step until the system is at rest. Since time is discretized, the simulation routine assumes a smaller force acting over the discretization interval instead of achieve $v_{t,i+1} = 0$ at the next time step, as sketched in Figure 3.

Soft contact models are generally better suited for optimization as discontinuities can be avoided. However, even in the absence of discontinuities, stiff contact models might introduce empirical bias, as mentioned above. The stiffness parameter thus trades off gradient quality with physical accuracy.

B. Discretization Artifacts

A further challenge of optimizing through contact is caused by discrete contact resolution. Most simulators detect contacts at the beginning of each time step, allowing for some interpenetration between detections. This can alter or invert the gradient direction compared to the continuous-time dynamics, as described in [3]. Note that decreasing the step size increases the accuracy of the forward simulation but does not improve the gradient for hard contact models.

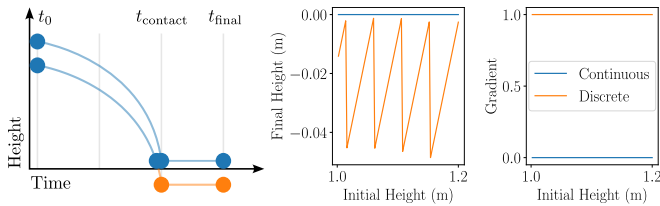


Fig. 4: Two falling spheres under gravity make inelastic contact with the ground. Blue lines depict the anticipated behavior in continuous time. The orange line illustrates the system’s behavior when discretized (left). Both contacts are resolved at time step t_c , resulting in discontinuous dynamics (middle). This obfuscates the gradient of the final height w.r.t. the initial height (right).

In [3], the ToI is computed with a linear model to correct for discretization artifacts. However, this is only accurate if the distance between the colliding bodies evolves linearly in time, which is generally not the case. Finding the exact ToI is not tractable without drastically increasing computation time. Against the common misconception, similar artifacts occur even without restitution, i.e., for inelastic collisions, as shown in Fig. 4.

The effect of ToI estimation on optimization is currently a subject of debate, with varying conclusions presented in recent studies [3], [4].

IV. CONTACT SIMULATION

We implement a differentiable rigid body simulator using Warp [13]. Our simulation advances the system dynamics in generalized coordinates and offers several contact models, serving as a platform for studying the importance of dynamics modeling for optimization.

A. Soft Contact

The first investigated contact model is based on penalty functions and is adopted from Warp’s predecessor dFlex, a differentiable physics engine also used in [5], rendering it an excellent baseline. At every time step, normal contact forces are computed according to

$$f_n = \begin{cases} k_p d - k_d \min(v_n, 0), & \text{if } d \geq 0 \\ 0, & \text{otherwise} \end{cases} \quad (5)$$

and tangential friction forces follow

$$\mathbf{f}_t = -\frac{\mathbf{v}_t}{\|\mathbf{v}_t\|_2} \min(k_f \|\mathbf{v}_t\|_2, \mu f_n), \quad (6)$$

where d is the penetration depth between the contacting bodies, \mathbf{v} is the relative velocity in the contact frame, and μ is the friction coefficient. The parameters k_p , k_d , and k_f have to be tuned and trade off physical accuracy against simulation stability and gradient smoothness. Inconveniently, the model behavior depends on various simulation parameters, such as the simulation step size or the mass of simulated objects. Note that the damping term of the normal force f_n introduces a discontinuity to the otherwise smooth model. However, damping is crucial to stabilize the simulation and

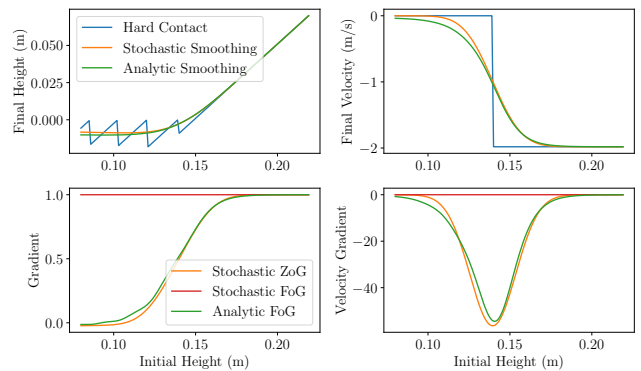


Fig. 5: The final height (top left), final velocity (top right), and their gradients (bottom) versus the initial height of a falling sphere under gravity. The sphere only collides with the ground if the initial height is small enough (left half of all graphs). Hard contact exhibits discontinuities in the position and velocity domain. Stochasticity helps to smooth discontinuities, but the FoG gradient is biased and uninformative. The analytically smoothed contact model induces similar effects on the dynamics as stochasticity, with the advantage of informative and unbiased FoGs.

to obtain more physically plausible results. After computing the contact forces, a semi-implicit Euler step evolves the system dynamics to the next time step.

B. Hard Contact

Next, we investigate a hard contact simulation routine based on Moreau’s time stepping scheme [26], similar to [27]. A key advantage over LCP-based simulation routines is that there is no need to linearize the friction cone. Additionally, the midpoint discretization used in Moreau’s scheme has slightly improved stability properties over semi-implicit Euler integration [28].

The implemented simulation routine begins with an explicit Euler half-step on position level that yields the position at the midpoint of the simulation step. Then, the Equation of Motion (EoM) is evaluated and contacts are resolved at the midpoint. The contact handling procedure determines the required impulses to satisfy all contact constraints at the end of the simulation step. It involves projecting parts of the EoM onto the contact domain and iterating over all contacts in a Gauss-Seidel fashion to converge to the appropriate impulses. A proximal projection ensures that contact forces always remain within the bounds of the friction cone. Finally, the dynamics are integrated using a midpoint rule.

Hard contact simulation is physically accurate but suffers from the phenomena described in Sec. III. Revisiting the introductory example of a falling, inelastic sphere exposes two discontinuities in the dynamics, shown in Fig. 5. The first discontinuity is observed in the sphere’s position, resulting from discrete time stepping. The second discontinuity, evident in the sphere’s velocity, originates from the discontinuity in the normal contact force, which propagates through the dynamics and becomes apparent in the velocity domain.

Algorithm 1 Modified Gauss-Seidel Iteration

Input: G, c, p, d, κ **Output:** p

```
for  $N$  solver iterations do
  for contact  $j \in C$  do
     $s \leftarrow \mathbf{0}$ 
     $r \leftarrow 0$ 
    for contact  $k \in C$  do
      if  $j = k$  then
         $s \leftarrow s + G_{jk} p_k$ 
      else
         $s \leftarrow s + G_{jk} p_k \cdot \text{sigmoid}(d_k, \kappa)$ 
         $r \leftarrow r + \det(G_{jk})$ 
     $r \leftarrow \frac{1}{1+r}$ 
     $p_j \leftarrow \text{prox}(p_j - r(s + c_j))$ 
 $p \leftarrow p \cdot \text{sigmoid}(d, \kappa)$ 
```

We additionally implement an optional ToI correction that approximates the ToI with a linear model, similar to [3], to investigate its importance in optimization.

C. Analytically Smoothed Contact

Stochastic smoothing effectively smoothes the discontinuities of hard contact but does not provide meaningful FoGs, as depicted in Fig. 5. Thus, we propose smoothing the hard contact model analytically to replicate the effects of stochasticity, similar to [8]. The contact model is smoothed by substituting the discontinuous step function, which represents the contact force in relation to the penetration depth, with a sigmoid function, as depicted in Figure 6². The smooth surrogate is defined as

$$\text{sigmoid}(d, \kappa) = \frac{1}{1 + e^{-d\kappa}}, \quad (7)$$

where κ determines the stiffness of the function.

Algorithm 1 outlines the modified Gauss-Seidel scheme for analytically smooth contact. Inputs to the contact solver are the Delassus Matrix G , which expresses the system’s inverse inertia in contact coordinates, c , which includes dynamic quantities that need to be counteracted by the contact impulses, and p , an initial guess for the impulses. The modified version additionally requires d , which contains the penetration depth for all active contacts, and κ . The iteration count N is fixed so that the solver loop can be unrolled during backpropagation. The set C contains all contacts that surpass a certain penetration depth³. In every iteration, a proximal operator projects the updated impulses onto the friction cone.

²While smoothing the step function with Gaussian noise, often employed to introduce stochasticity in RL methods, would yield the error function [1], this work relies on the sigmoid function for its lower computational cost. The sigmoid function is equivalent to the step function smoothed with logistic noise [8].

³The threshold should be chosen to limit the number of active contacts and thus computational cost. We set the threshold to -1 m and only consider foot contacts.

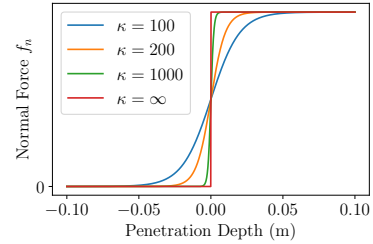


Fig. 6: The analytically smoothed contact model. The discontinuous step function of the normal contact force f_n is replaced with a sigmoid function. Different stiffness parameters κ control the smoothing intensity. A value of $\kappa = \infty$ recovers the original hard contact model.

Similar to RL algorithms, the level of stochasticity or smoothness can be incrementally reduced during the training process to shift towards a more precise model by adjusting κ . The model can become arbitrarily stiff without destabilizing the simulation, a significant advantage over the previously introduced soft contact model.

V. RESULTS

We compare the introduced contact models for the task of quadrupedal locomotion, which requires making and breaking contact frequently. The learning setup is detailed in the Appendix. We employ SHAC [5], an optimization algorithm that demonstrates potential in optimizing contact-rich tasks. SHAC is a mixed-order method, using FoGs over a short horizon and ZoGs to approximate the future return after the short horizon trajectory via a value function. This approach effectively avoids gradient divergence by only backpropagating through trajectories with a relatively small number of transitions. Additionally, the value function smooths the optimization landscape, combating the discussed issues in optimizing discontinuous functions. Qualitative results of the emerging locomotion behaviors can be seen in the supplementary video.

A. The Effects of Contact Modeling

As shown in Fig. 8, all contact models result in similar convergence properties during optimization. The penalty-based contact model yields the highest reward. However, the model yields poor results in terms of physical accuracy and permits the largest penetration into the ground, as depicted in Fig. 7. More critically, policies take advantage of the ground’s spring-like properties, resulting in trampoline-like jumping movements, as outlined in Fig. 1, which explain the higher reward obtained. Making the soft model more precise by increasing its stiffness is not feasible, as the gradient norm quickly grows and diverges.

To investigate if learned policies transfer to more physically realistic environments, a policy is executed using the hard contact model. As anticipated, the robot quickly loses balance and falls after a few time steps. To conclude, the investigated soft contact model features properties that

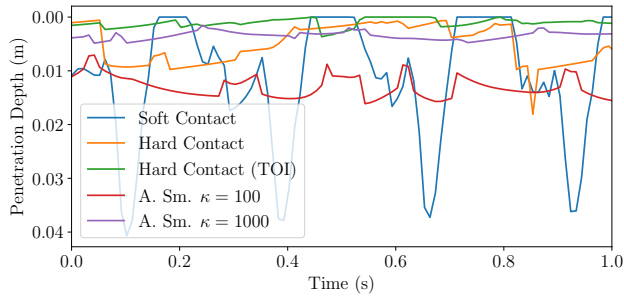


Fig. 7: The mean penetration depth d of all contacts during locomotion for different contact models. Using the penalty-based model results in the largest contact constraint violation. ToI correction significantly reduces the penetration depth over hard contact without ToI estimation. The analytically smooth contact model varies depending on κ , but can achieve small violations if κ is chosen large enough.

facilitate efficient optimization, explaining its use in recent works [6], [5]. However, its lack of accuracy does not allow for transfer to the physical world, rendering it unsuitable for robotics tasks.

For more physically accurate results, employing a hard contact model appears to be essential⁴. Interestingly, optimization is successful despite the discontinuities depicted in Fig. 5, suggesting that the employed algorithm effectively smooths the optimization landscape.

Nevertheless, policies trained with hard contact sometimes exhibit unnatural walking behaviors involving suboptimal foothold locations. This is likely due to misleading gradients arising from discontinuities. Augmenting the simulation with ToI estimation holds little improvement, in line with the findings of [4]. A linear approximation is possibly too inaccurate to effectively mitigate the discretization artifacts. In general, the effect of ToI estimation is expected to be more pronounced when training with purely FoG-based methods.

The benefits of the analytically smoothed contact model are not reflected in the learning curves, where its performance is comparable to the hard contact model, but the resulting locomotion behaviors are significantly smoother and lack the previously observed erratic footholds. To test the contact model’s effectiveness, policies are re-executed in a hard contact simulation. Notably, policies are effectively transferred, even if they were trained with a relatively smooth model, e.g., for $\kappa = 100$. This confirms the intuition that the characteristic of stochastic smoothing, which maintains the deterministic case within its domain, is effectively replicated by the introduced analytic smoothing method.

Scheduling the smoothness during training promises even better transferability, as the final model is closer to hard contact. Emerging behaviors still feature smooth motions, making this method the most promising among those examined for effective real-world deployment.

⁴To ensure stable gradients with hard contact simulation, armature is added to the diagonal elements of each body’s inertia matrix.

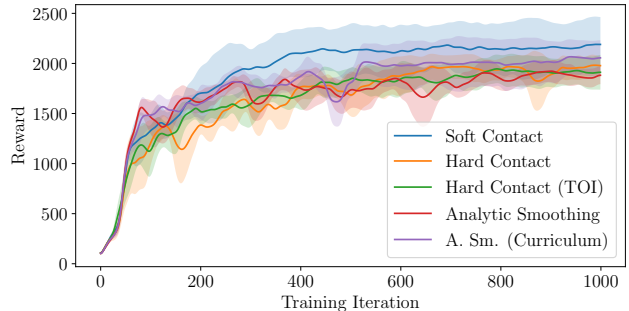


Fig. 8: The mean total reward received during a task episode for different contact models over the course of training. The reward is averaged over five training runs with different random seeds (0 to 4), and the standard deviation is indicated by the shaded regions.

B. A Comparison to PPO

We compare SHAC to the publicly available PPO implementation RSL RL [10]. Both algorithms exhibit analogous convergence properties and achieve nearly identical final rewards, as shown in Figure 9. Nevertheless, SHAC outperforms PPO in terms of sample efficiency, owing to the reduced variance of ZoGs. Primarily, this leads to reduced memory requirements during the training process. Providing a fair comparison in terms of time complexity is challenging because training duration also hinges on the particular implementation details. In the implementations discussed in this thesis, a single training iteration for SHAC takes roughly 0.5 s and for PPO about 1 s.

VI. CONCLUSIONS

This paper explored the effect of contact modeling on FoG-based optimization for the contact-rich task of learning quadrupedal locomotion. We demonstrated the feasibility of attaining walking behaviors with hard contact, offering a physically more accurate approach than penalty-based models [5]. Our analytically smooth contact formulation led to improved movement fluency, while the resulting policies successfully transferred to hard contact simulation. A comparison of SHAC and PPO showed that although both algorithms converge at a similar rate and to a comparable optimum, SHAC did so with notably higher sample efficiency.

Future research could aim to reduce the dependency on ZoGs, currently still included through the use of a value function, to further enhance sample efficiency. The proposed contact model’s ability to smooth discontinuities reduces the necessity of the value function’s smoothing effect. Another promising path could involve exploring more complex tasks currently beyond the reach of RL methods, where FoG-based strategies might succeed. Finally, confirming the real-world applicability of policies trained with the proposed method remains an important step we plan to address in future work.

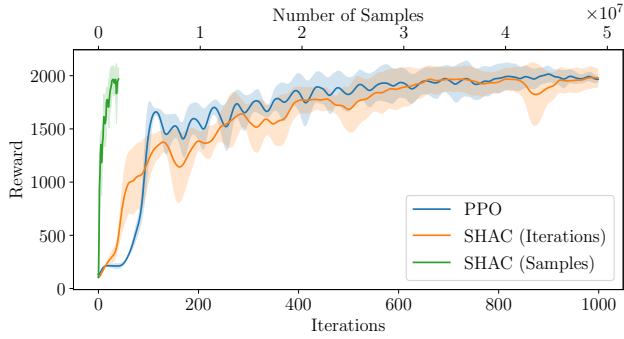


Fig. 9: The mean total reward received during a task episode for the algorithms SHAC and PPO throughout training in terms of iterations and number of samples. The reward is averaged over five training runs with different random seeds (0 to 4), and the standard deviation is indicated by the shaded regions. Both algorithms are evaluated using the hard contact simulation.

APPENDIX

Table II specifies the used rewards. The control policy outputs position commands for the joints that are tracked with a PD-control law. The maximum torque applied by the actuators is 20 Nm. Environments are terminated if the center of the quadruped’s base falls below 0.25 m with respect to the ground or if the maximum episode length of 10 s is reached. Contact models are evaluated using the parameters $k_p = 12 \cdot 10^3$, $k_d = 3$, $k_f = 9 \cdot 10^2$ for the spring-damper model, $\kappa = 100$ for the analytically smoothed model, and $\kappa = 100 \rightarrow 1000$ for the analytically smoothed model with a curriculum if not stated otherwise.

TABLE II: Rewards

Name	Formula	Weight
Base velocity	$\exp(\dot{x}_{\text{base}} - 1.0)$	1.0
Base height	$\exp((y_{\text{base}} - 0.45))$	0.5
Base alignment	$e^{\text{world}} \cdot e^{\text{base}}$	0.5
Actions	$\sum_i \exp(- a_i)$	0.01
Joint velocity	$-\ \dot{q}_{\text{joints}}\ ^2$	0.001

REFERENCES

- [1] H. J. Suh, M. Simchowitz, K. Zhang, and R. Tedrake, “Do differentiable simulators give better policy gradients?” in *International Conference on Machine Learning*. PMLR, 2022, pp. 20 668–20 696.
- [2] J. Degraeve, M. Hermans, J. Dambre, and F. Wyffels, “A differentiable physics engine for deep learning in robotics,” *Frontiers in Neuro-robotics*, vol. 13, no. March, pp. 1–9, 2019.
- [3] Y. Hu, L. Anderson, T.-M. Li, Q. Sun, N. Carr, J. Ragan-Kelley, and F. Durand, “DiffTaichi: Differentiable programming for physical simulation,” in *ICLR*, 2019.
- [4] C. D. Freeman, E. Frey, A. Raichuk, S. Girgin, I. Mordatch, and O. Bachem, “Brax-a differentiable physics engine for large scale rigid body simulation,” in *Thirty-fifth Conference on Neural Information Processing Systems Datasets and Benchmarks Track (Round 1)*, 2021.
- [5] J. Xu, V. Makoviychuk, Y. Narang, F. Ramos, W. Matusik, A. Garg, and M. Macklin, “Accelerated policy learning with parallel differentiable simulation,” in *International Conference on Learning Representations*, 2021.

- [6] M. Geilinger, D. Hahn, J. Zehnder, M. Bächer, B. Thomaszewski, and S. Coros, “ADD: Analytically differentiable dynamics for multi-body systems with frictional contact,” *ACM Transactions on Graphics*, vol. 39, no. 6, 2020.
- [7] J.-J. Moreau, “Some basics of unilateral dynamics,” in *IUTAM Symposium on Unilateral Multibody Contacts*. Springer, 1999, pp. 1–14.
- [8] T. Pang, H. J. Suh, L. Yang, and R. Tedrake, “Global Planning for Contact-Rich Manipulation via Local Smoothing of Quasi-Dynamic Contact Models,” *IEEE Transactions on Robotics*, pp. 1–20, 2023.
- [9] J. Schulman, F. Wolski, P. Dhariwal, A. Radford, and O. Klimov, “Proximal policy optimization algorithms,” *arXiv e-prints*, 2017.
- [10] N. Rudin, D. Hoeller, P. Reist, and M. Hutter, “Learning to walk in minutes using massively parallel deep reinforcement learning,” in *Conference on Robot Learning*. PMLR, 2022, pp. 91–100.
- [11] F. d. A. Belbute-Peres, K. R. Allen, K. A. Smith, J. B. Tenenbaum, and J. Zico Kolter, “End-to-end differentiable physics for learning and control,” *Advances in Neural Information Processing Systems*, pp. 7178–7189, 2018.
- [12] K. Werling, D. Omens, J. Lee, I. Exarchos, and C. K. Liu, “Fast and Feature-Complete Differentiable Physics for Articulated Rigid Bodies with Contact,” *Robotics: Science and Systems*, 2021.
- [13] M. Macklin, “Warp: A high-performance python framework for gpu simulation and graphics,” <https://github.com/nvidia/warp>, March 2022, .NVIDIA GPU Technology Conference (GTC).
- [14] M. Macklin, M. Müller, and N. Chentanez, “Xpbd: position-based simulation of compliant constrained dynamics,” in *Proceedings of the 9th International Conference on Motion in Games*, 2016, pp. 49–54.
- [15] E. Todorov, T. Erez, and Y. Tassa, “Mujoco: A physics engine for model-based control,” *2012 IEEE/RSJ International Conference on Intelligent Robots and Systems*, pp. 5026–5033, 2012.
- [16] T. A. Howell, S. Le Cleac’h, J. Z. Kolter, M. Schwager, and Z. Manchester, “Dojo: A differentiable simulator for robotics,” *arXiv preprint arXiv:2203.00806*, vol. 9, 2022.
- [17] Z. Huang, Y. Hu, T. Du, S. Zhou, H. Su, J. B. Tenenbaum, and C. Gan, “Plasticinelab: a Soft-Body Manipulation Benchmark With Differentiable Physics,” *ICLR 2021 - 9th International Conference on Learning Representations*, pp. 1–18, 2021.
- [18] S. Le Cleac’h, H. X. Yu, M. Guo, T. Howell, R. Gao, J. Wu, Z. Manchester, and M. Schwager, “Differentiable Physics Simulation of Dynamics-Augmented Neural Objects,” *IEEE Robotics and Automation Letters*, vol. 8, no. 5, pp. 2780–2787, 2023.
- [19] J. K. Murthy, M. Macklin, F. Golemo, V. Voleti, L. Petrini, M. Weiss, B. Considine, J. Parent-Lévesque, K. Xie, K. Erleben *et al.*, “gradsim: Differentiable simulation for system identification and visuomotor control,” in *ICLR*, 2020.
- [20] D. Turpin, L. Wang, E. Heiden, Y.-C. Chen, M. Macklin, S. Tsogkas, S. Dickinson, and A. Garg, “Grasp’d: Differentiable contact-rich grasp synthesis for multi-fingered hands,” in *European Conference on Computer Vision*. Springer, 2022, pp. 201–221.
- [21] R. Antonova, J. Yang, K. M. Jatavallabhula, and J. Bohg, “Rethinking optimization with differentiable simulation from a global perspective,” in *Conference on Robot Learning*. PMLR, 2023, pp. 276–286.
- [22] H. J. T. Suh, T. Pang, and R. Tedrake, “Bundled Gradients Through Contact Via Randomized Smoothing,” *IEEE Robotics and Automation Letters*, vol. 7, no. 2, pp. 4000–4007, 2022.
- [23] N. Wiedemann, V. Wüest, A. Loquercio, M. Müller, D. Floreano, and D. Scaramuzza, “Training efficient controllers via analytic policy gradient,” in *2023 IEEE International Conference on Robotics and Automation (ICRA)*. IEEE, 2023, pp. 1349–1356.
- [24] M. A. Z. Mora, M. Peychev, S. Ha, M. Vechev, S. Coros, M. Zamora, M. Peychev, S. Ha, M. Vechev, and S. Coros, “PODS: Policy Optimization via Differentiable Simulation,” *38th International Conference on Machine Learning*, pp. 7805–7817, 2021.
- [25] Y. L. Qiao, J. Liang, V. Koltun, and M. C. Lin, “Efficient Differentiable Simulation of Articulated Bodies,” *Proceedings of Machine Learning Research*, vol. 139, pp. 8661–8671, 2021.
- [26] J. J. Moreau, “Unilateral contact and dry friction in finite freedom dynamics,” in *Nonsmooth mechanics and Applications*. Springer, 1988, pp. 1–82.
- [27] J. Carius, R. Ranftl, V. Koltun, and M. Hutter, “Trajectory optimization with implicit hard contacts,” *IEEE Robotics and Automation Letters*, vol. 3, no. 4, pp. 3316–3323, 2018.
- [28] J. Bender, K. Erleben, and J. Trinkle, “Interactive simulation of rigid body dynamics in computer graphics,” *Computer Graphics Forum*, vol. 33, no. 1, pp. 246–270, 2014.